Biomass Conversion and Biorefinery (2018) 8:889–897
https://doi.org/10.1007/s13399-018-0329-3

ORIGINAL ARTICLE

Valorization of humins by phosphoric acid activation for activated carbon production

Shimin Kang[1] · Shaohui Jiang[1] · Zhezhe Peng[1] · Yue Lu[2] · Jianfeng Guo[1] · Jianwen Li[1] · Wanxiang Zeng[1] · Xiaoyuan Lin[1]

Received: 17 May 2018 / Revised: 4 July 2018 / Accepted: 18 July 2018 / Published online: 11 September 2018

Abstract

Humins, the solid wastes from biomass acid hydrolysis, were value-added applied for activated carbon production through the phosphoric acid activation method with pyrolysis temperature ranging from 300 to 700 °C. Studies on structure and properties found that pyrolysis temperature is a key factor affecting pore formation of activated carbons. A good yield of 51.4 wt%, high BET surface area of 2375 m^2/g, Barrett-Joyner-Halenda (BJH) pore volume of 0.88 cm^3/g, and an excellent Langmuir adsorption capacity of 1125 mg/g on methylene blue (MB) were obtained under the preferred temperature of 400 °C (AC400). The adsorption of MB was well explained by the pseudo-second-order kinetic model, and the adsorption behavior complied with Langmuir isotherm model. Dichloromethane (DCM) was found a most effective extractant in AC400 regeneration by using Soxhlet apparatus. A comparable adsorption capacity of 680 mg/g MB was maintained for the fifth reusing of the AC400, illustrating the application potential of humins valorization for biomass residues recycling industry.

Keywords Humins · Biomass hydrolysis · Activated carbon · Methylene blue

1 Introduction

Production of top platform chemicals, such as levulinic acid and 5-hydroxymethylfurfural, from cellulosic biomass acid-catalyzed hydrolysis has attracted much attention [1]. Both levulinic acid and 5-hydroxymethylfurfural can be converted into value-added chemical intermediates, fuels, polymers, solvents, and resins [1]. Levulinic acid was even regarded as a chemical bridge connecting biomass and petroleum processing, due to its importance in producing a variety of liquid biofuels (e.g., valerate esters, γ-valerolactone, liquid alkenes) [2, 3]. Humins, the solid wastes, are inevitably generated during the biomass acid hydrolysis process, leading to serious decreases of biomass utilization efficiency [4]. The humin yields reached 21–36 wt% from glucose acid hydrolysis for production of levulinic acid and/or 5-hydroxymethylfurfural [5–9], and as high as 30–50 C% during levulinic acid production from cellulose hydrothermal conversion [10]. It is meaningful to develop high value-added products from waste humins for the whole biorefineries. Several works have focused on conversion of humins to bio-oils [11], syngas [12], organic acids [13], and composites and polymeric materials [14, 15]. Importantly, the humins are stable polymer containing 50–66% carbon [9, 13, 16, 17]. The carbon rich in property and polymer structure made humins a potential feedstock for production of porous carbon materials, e.g., activated carbons [18]. For comparison, terrestrial higher plants are routine materials for activated carbon production, while their average carbon content is only about 44% [19]. Activated carbons are widely applied in manufacturer and our daily life, such as wastewater treatment, air clean, and detoxification agent for biomass hydrolysate [20, 21]. They could be prepared through several technologies, in which chemical activation is the most conventional one with alkali (e.g., KOH), salt (e.g., $ZnCl_2$), and acid (H_3PO_4) [22, 23] as the activating agents.

As humins are formed from acid-catalyzed polymerization reactions, the use of acidic activating agent (e.g., H_3PO_4) might avoid excessive corrosion of humins carbon structure,

✉ Yue Lu
luyue2017@mail.xhu.edu.cn

[1] Guangdong Provincial Key Laboratory of Distributed Energy Systems, Dongguan University of Technology, Dongguan, Guangdong, China

[2] School of Food and Biological Engineering, Xihua University, Chengdu, China

which would give a high yield of activated carbon. In addition, a part of the mineral acid used for acid hydrolysis could be adsorbed on raw humins [5]. The use of acidic activating agent does not require the neutralization reaction or excessive water washing to remove acids before the activation process.

To make waste humins profitable, H_3PO_4 activation and pyrolysis process were originally determined for activated carbon production from humins. The structure and properties of the activated carbons were systematically investigated, and the performances were elaborated by adsorption of methylene blue (MB), a common dye contaminant.

2 Materials and methods

2.1 Materials

Humins were obtained by a routine H_2SO_4 (0.05 mol/L) catalytic hydrolysis process [13]. In brief, 80 mL of acidic glucose solution (1 mol/L) was put in a 100-mL unstirred polytetrafluoroethylene reactor, and then the reactor was sealed and heated in an oven. After 1 h of heating time, the reactor reached 160 °C and then kept at the temperature for 6 h. After reaction and cooling down, the solids were filtrated, washed, and dried at 100 °C to obtain humins. Methylene blue (MB) was purchased from Macklin Reagent, Shanghai, China.

2.2 Activation treatments

In the activation process, 3.0 g of humins was mixed with 20 mL 40% H_3PO_4 solution and stirred for 12 h, and the slurry was further oven dried at 120 °C for 12 h. The dried sample was heated to a preset temperature (300–700 °C) with a heating rate of 10 °C/min in a horizontal cylindrical furnace, and then kept at the preset temperature for 2 h with nitrogen protection (100 mL/min nitrogen flushing rate). The prepared samples were washed repeatedly with DI water until the pH level is back to 7. The sample was dried at 120 °C for 12 h to obtain activated carbon and, labeled as AC*X* according to each pyrolysis temperature *X*. For example, the activated carbon prepared at 400 °C is labeled as AC400.

2.3 Sample characteristics

The morphology of the samples was analyzed by a JEOL JSM-6701F environmental scanning electron microscopy (SEM) system (Tokyo, Japan). The functional groups were analyzed by Fourier transform infrared spectroscopy (FT-IR) (Bruker Tensor 27, Karlsruhe, Germany) using KBr as an interference-free matrix. The samples were mixed and ground with KBr by a ratio of 1:10, and the scanning region ranged from 1000 to 3600 cm^{-1}. X-ray diffraction (XRD) was analyzed by a Rigaku D/max-IIIA X-ray diffractometer (TX, USA). Thermogravimetric (TG) analyses were conducted by a Netzsch 209F3 (NETZSCH-Gerätebau GmbH, Germany). The ACs were placed in a sample pan under air and heated from room temperature to 600 °C with a heating rate of 10 °C/min. The nitrogen adsorption–desorption isotherms were analyzed by a Micromeritics Instruments TriStar II (GA, USA) to evaluate the Brunauer–Emmett–Teller (BET) surface area and total Barrett, Joyner, and Halenda (BJH) pore volume with pores from 1.7 to 300 nm. AC400 was also analyzed by an Autosorb-iQ-C chemisorption–physisorption analyzer (Quantachrome, USA) in order to measure the micropores with diameter < 1.7 nm. All the texture characteristics of the ACs were determined by low-temperature (77.4 K) nitrogen adsorption with the addition of 0.07–0.1 g sample in the quartz testing tube. The total acid groups were determined by the Boehm titration method [24]. Briefly, the ACs were added into 0.02 mol L^{-1} NaOH solution in a glass bottle, and the bottle was shaken in a shaking bed for 24 h. After shaking and filtration, a pre-prepared amount of HCl solution (0.03 mol/L) was added to the solution. Then, the solution was back-titrated with NaOH solution (0.02 mol L^{-1}) to neutral using phenolphthalein as an indicator.

2.4 Adsorption and desorption process

Adsorption of MB was performed in 50-mL sealed glass bottles. Thirty milliliters solution with initial concentration of 1000–2000 mg/L was placed without any pH adjustment. Fifty-milligram humins-based activated carbon was added into each bottle and placed in an isothermal shaker at 200 rpm and 30 °C for 24 h. After each adsorption process, the MB solution was separated from the activated carbon by filtration, and the MB concentration was analyzed by UV-vis spectrum analysis at 663 nm.

The regeneration of used AC400 was conducted by organic solvent extraction in a 60-mL Soxhlet extractor. The AC400 (50 mg) was first shaken with 2000 mg/L MB solution for 24 h. The MB-adsorbed AC400 was put in the Soxhlet extractor, and then extracted by three common organic solvents, i.e., methanol, acetone, dichloromethane (DCM) for 24 h. The volatilization temperature of the methanol, acetone, and DCM in the bottom of the Soxhlet extractor was 75 °C, 70 °C, and 55 °C, respectively. After the extraction process, the treated AC400 was dried at 45 °C to evaporate the organic solvents to obtain the regenerated AC400. The regenerated AC400 was reused for MB adsorption as described above.

2.5 Simulation and calculation

Two generally used kinetic models, pseudo-first-order and pseudo-second-order, were used for the kinetic dynamic

simulation. The linear form of pseudo-first-order rate is shown in Eq. (1):

$$\ln(q_e - q_t) = \ln q_e - k_1 t \quad (1)$$

The linear form of pseudo-second-order rate is shown in Eq. (2):

$$\frac{t}{q_t} = \frac{1}{k_2 q_e^2} + \frac{t}{q_e} \quad (2)$$

where q_t and q_e is the amount of MB adsorbed on the sorbent at time (min) and at equilibrium (mg/g), respectively. k_1 is the first-order rate constant (h^{-1}) and k_2 is the pseudo-second-order rate constant (g/mg min).

The kinetics parameters and correlation coefficients (R^2) were determined by linear regression. The applicability of both kinetic models was verified by normalized standard deviation Δq (%) as shown in Eq. (3):

$$\Delta q\,(\%) = 100 \times \sqrt{\sum \frac{\left[\frac{q_{exp} - q_{cal}}{q_{exp}}\right]^2}{(n-1)}} \quad (3)$$

where the subscripts "exp" and "cal" refer to the experimental and calculated values, respectively, and n is the number of data points.

Two adsorption models, Langmuir and Freundlich models, were used to simulate the adsorption process [25]. The linearized Langmuir isotherm is shown as Eq. (4):

$$\frac{C_e}{q_e} = \frac{1}{q_m K_L} + \frac{1}{q_m C_e} \quad (4)$$

where K_L is the Langmuir constant (L/mg).

The linearized Freundlich isotherm is shown as Eq. (5):

$$\ln q_e = \ln K_F + \frac{1}{n_F \ln C_e} \quad (5)$$

here the n_F is used to indicate whether the adsorption is linear, or a typical chemical or a favorable physical process, and the K_F is the Freundlich constant.

An equilibrium parameter R_L (Eq. (6)) was used to interpret the adsorption process, whether it is "favorable" or not.

$$R_L = \frac{1}{1 + K_L C_0} \quad (6)$$

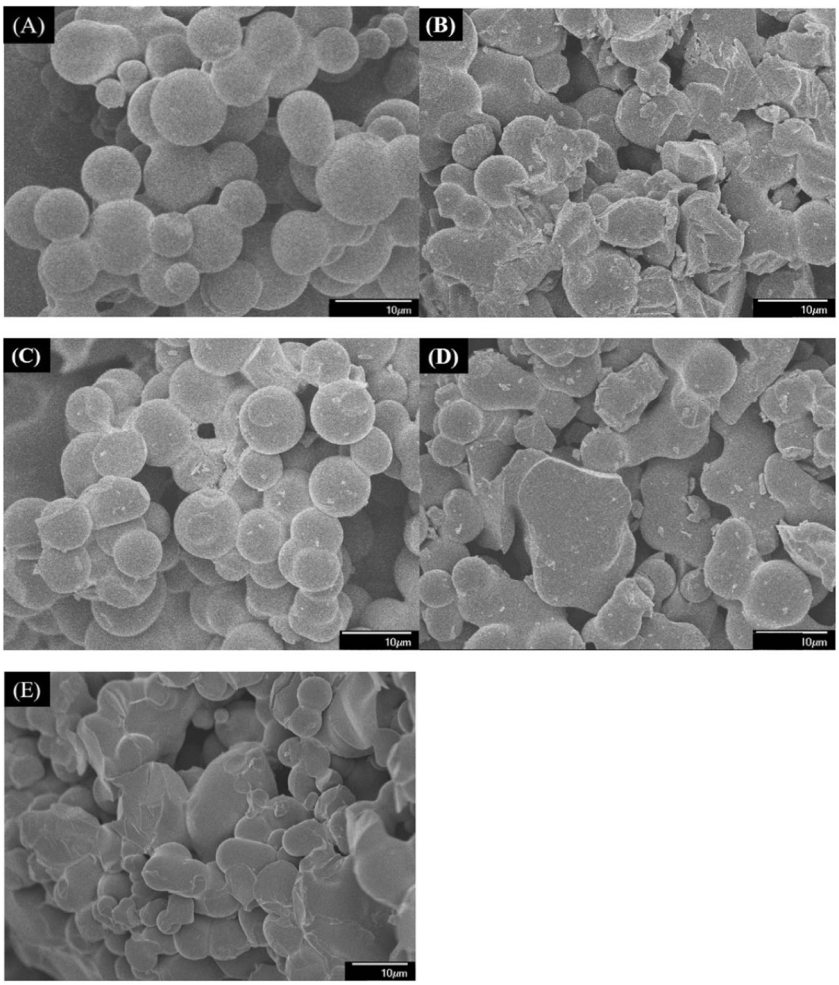

Fig. 1 SEM images of humins (**a**), AC400 (**b**), AC500 (**c**), AC700 (**d**), and MB-adsorbed AC400 (**e**)

Table 1 Properties of humins and activated carbons

Sample	Yields (wt%)	BET surface area (m^2/g)	BJH pore volume[a] (cm^3/g)	Total acidity (meq g^{-1})	MB adsorption capacity (mg g^{-1})[b]
Humins	–	6	Negligible	–	–
Humins400[c]	77.2	39	< 0.01	–	–
AC300	73.5	1358	0.25	3.7	865
AC400	51.4	2375	0.88	3.6	1085
AC500	65.3	2005	0.83	3.4	1061
AC600	55.0	1774	0.41	3.4	1052
AC700	51.9	1673	0.35	3.3	1059
MB-adsorbed AC400[d]	–	862	0.27	–	–

[a] Measured between 1.7-nm and 300-nm width

[b] 0.05 g of activated carbon used for adsorption in 30 mL 2000 mg/L MB solution for 24 h

[c] The solid products from humins pyrolysis at 400 °C for 2 h

[d] 0.05 g of AC400 used for adsorption in 30 mL 2000 mg/L MB solution for 24 h

3 Results and discussion

3.1 Characteristics of activated carbons

The humins were solid residues cumulated by microspheres with a diameter of 2–10 nm (see Fig. 1a), with a very low BET surface area (6 m^2/g) and negligible pore volume (see Table 1). Direct pyrolysis of humins at 400 °C only resulted in a carbon material with a still low BET surface area of 39 m^2/g and pore volume (see Table 1), indicating low contents of pores were formed. As expected, the H_3PO_4 activation promoted the formation of pores, and a high BET surface area of 2375 m^2/g was measured on the AC400. The H_3PO_4 would apply as an acid catalyst promoting bond cleavage and crosslinks formation, and form phosphate and polyphosphate bridges connecting and crosslinking polymer fragments [26, 27]. Because of the dilation process caused by the addition and/or insertion of phosphate groups, pore structures were formed in the matrix in an expanded state after the removal of acid. However, phosphate linkages is thermally unstable at temperature above 450 °C, which lead to form an activated carbon with more densely packed and less porous structure [26, 27]. In addition, H_3PO_4 is instable over high temperatures of 213 °C (http://www.ilo.org/dyn/icsc/showcard.display?p_version=2&p_card_id=1008, http://erplan.net/msds/7664382msds.htm). With the increase of temperature, H_3PO_4 would lose water to form pyrophosphoric acid (e.g., 200–300 °C) and further lose water to form triphosphoric acid

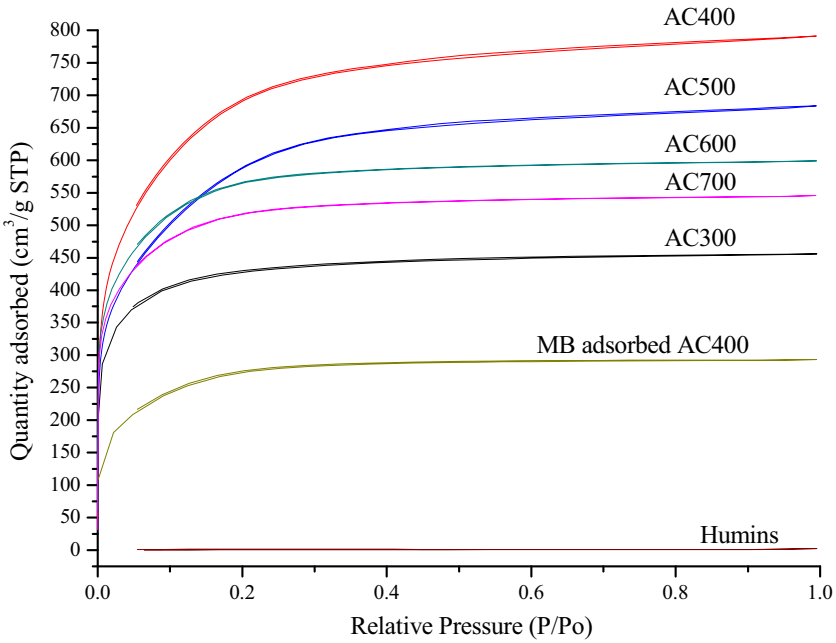

Fig. 2 Nitrogen adsorption isotherms for various activated carbons at 77 K

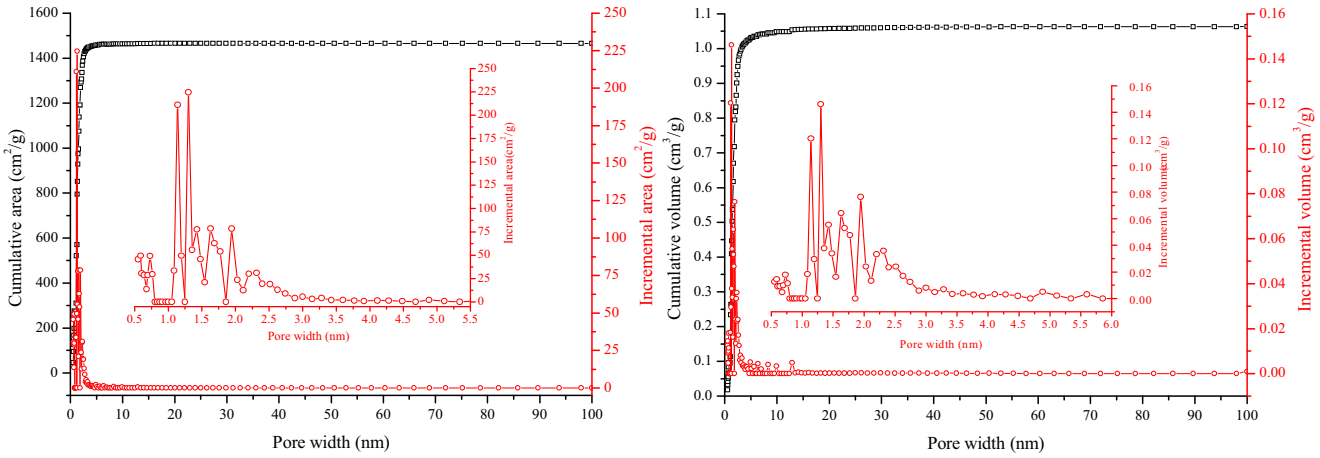

Fig. 3 Pore size (0.5–100 nm) distribution of AC400

and even partial phosphoric acid (e.g., > 300 °C) [28, 29]. The loss of water in the H_3PO_4 body with the increase of temperature might affect the acid catalytic activity. Therefore, the properties of activated carbons should be affected by both the H_3PO_4 activation effects and pyrolysis temperature. As shown in Fig. 1, the microspheres of activated carbons were destroyed on the AC400. Interestingly, microspheres were still on AC500, though a small

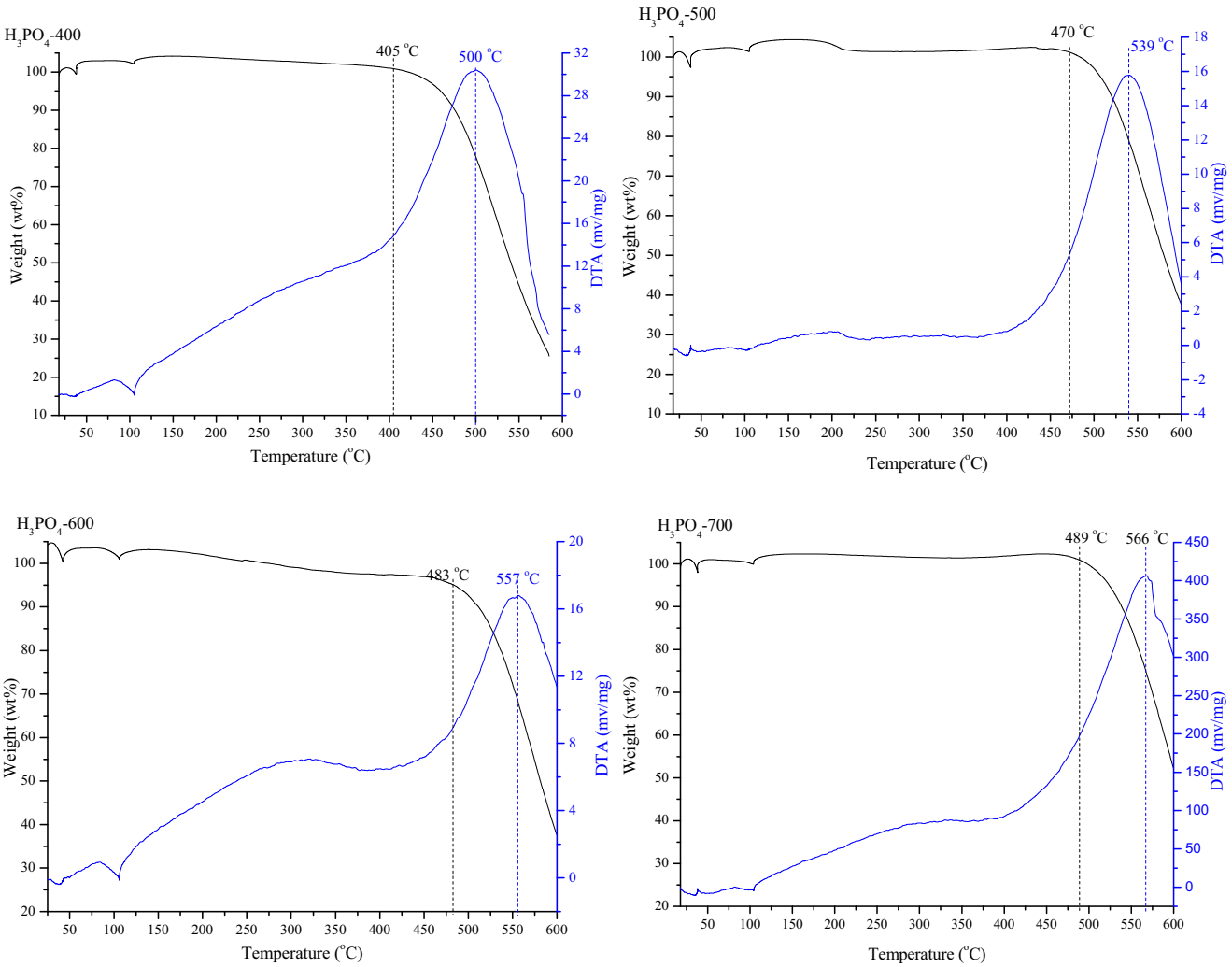

Fig. 4 Thermal stability of AC400–AC700 in air atmosphere

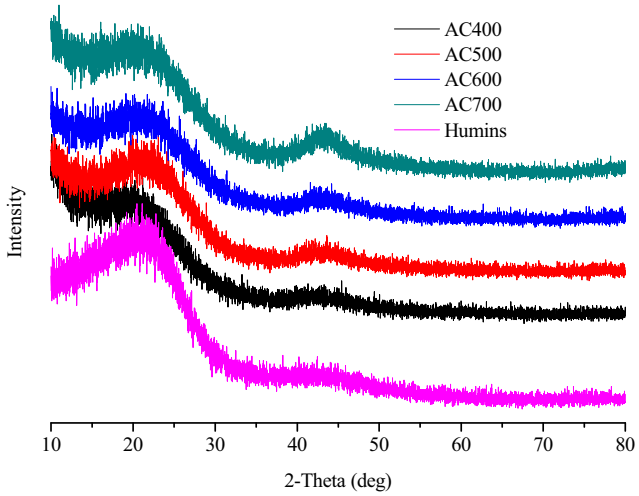

Fig. 5 XRD spectra of humins and AC400–AC700

destruction of these microspheres was observed. However, the destruction of the microspheres was observed again on the AC700. In addition, the AC500 had relative higher yields than AC400 and AC700, and had similar microspheres to that of humins, indicating both H_3PO_4 activation effects and direct pyrolysis were relatively weak at 500 °C. It seemed that the H_3PO_4 activation effects caused a most serious destruction of humins at 400 °C, while high-temperature pyrolysis resulted in microsphere destruction at 700 °C. Since H_3PO_4 activation effects were key factors for the formation of pores, a high pyrolysis temperature may not be favored due to the instability of H_3PO_4 and phosphate linkages. This is confirmed by BET surface area and total pore volume data as listed in Table 1. For example, the trend of surface area is AC400 (2375 m^2/g) > AC500 (2005 m^2/g) > AC600 (1774 m^2/g) > AC700 (1673 m^2/g). It is noted a very low pyrolysis temperature of 300 °C could not effectively promote the pore formation, as the AC300 has a relative low surface area of 1358 m^2/g.

The N_2 adsorption isotherms at 77 K for AC300–AC700 are shown in Fig. 2. All the isotherms belong to IUPAC type I isotherm, and a sharp curve of increased adsorption volume was observed at relatively low pressures ($P/P_0 < 0.2$), indicating the adsorption was mainly contributed by small pores. The pore size distribution of AC400 is shown in Fig. 3, which confirms the major surface area and pore volumes are attributed to the pores with diameter ≤ 3 nm. Actually, the average diameter of AC400 was 1.97 nm.

It is very common to use activated carbon in the presence of air. The thermal stability investigation of AC400–AC700 under air atmosphere is shown in Fig. 4. The TG inflection temperature and the highest DTA temperature peak of AC400, AC500, AC600, and AC700 were around 405 and 500 °C, 470 and 539 °C, 483 and 557 °C, 489 and 566 °C, respectively. Therefore, all the AC400–AC700 might be used below 400 °C, and a higher activation temperature benefits for the thermal stability. The humins and all the AC400–AC700 are amorphous carbon, based on broad diffraction peaks located between $2\theta = 15°$ and 30° in the XRD spectra (see Fig. 5) [24]. The FT-IR spectra (Fig. 6) indicated the formation of aromatic groups in the pyrolysis process, since the AC400 has much stronger peaks around 1540 and 1590 cm^{-1} as compared with the humins. The AC400 also has a hydroxyl group (around 3440 cm^{-1}) and C=O bond (around 1820 cm^{-1}), which are important acidic groups in favor of adsorption of alkaline solutes (e.g., MB). Actually, the acidic groups of the AC300–AC700 were between 3.3 and 3.7 mmol/g as listed in Table 1.

3.2 Adsorption

3.2.1 Adsorption comparison and mechanism

To compare the adsorption capability, all the AC300–AC700 were used to adsorb MB with an initial concentration of 2000 mg/L for 24 h, and the AC400 exhibited the highest MB adsorption capability (1085 mg/g) as listed in Table 1. This highest adsorption capability of AC400 can be attributed

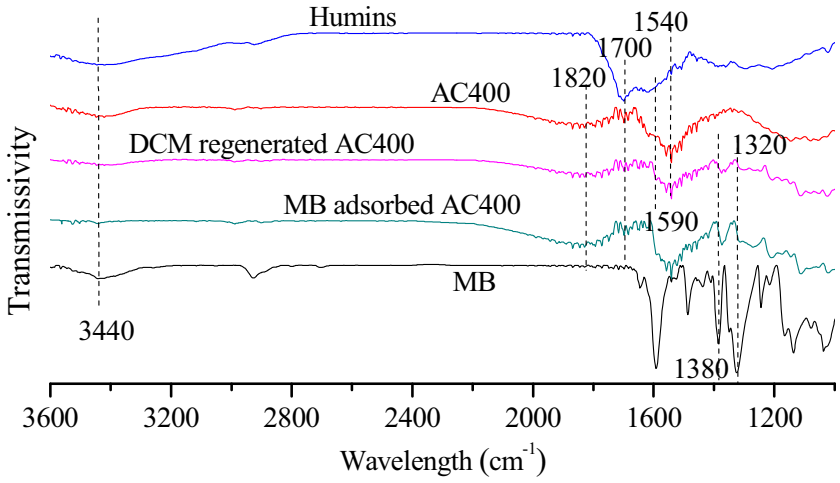

Fig. 6 FT-IR spectra of humins, MB, AC400, MB-adsorbed AC400, and DCM-regenerated AC400

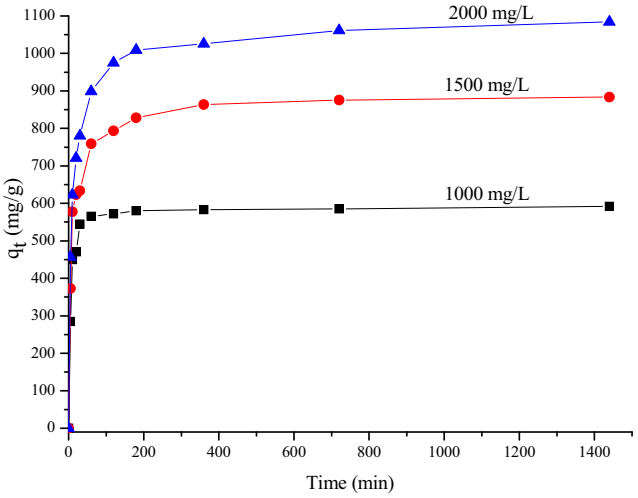

Fig. 7 Adsorption isotherms of MB with various concentrations

to its highest surface area and total pore volumes (see Table 1). The BET surface area and total BJH pore volume with pore size 1.7–300 nm on AC400 decreased from 2375 m^2/g and 0.88 cm^3/g to 862 m^2/g and 0.27 cm^3/g, respectively, after the adsorption process. Since the pore volume of MB is negligible, the decrease of total BJH pore volume means that about 0.317 (=0.88−(1 + 1.085) × 0.27) cm^3 of the initial pore volume with aperture1.7–300 nm per gram AC400 was filled by the MB. The three-dimension of MB is 1.41-nm width, 0.55-nm depth, and 0.16-nm thickness, respectively [30], and the molecular volume of MB is 0.297 nm^3. Therefore, about 1.07×10^{21} MB molecules (or 566 mg) were adsorbed by the pores with 1.7–300 nm. It was reported an accessible pore size for dye adsorption should be at least 1.3–1.8 times greater than the dye molecule width [31]. Therefore, the adsorption of MB on micropores with aperture < 1.7 nm might be negligible in considering the width of MB (1.41 nm). The adsorption of the rest 47.8% ($=\frac{1085-566}{1085} \times 100\%$) of MB (519 mg) per gram AC400 was mainly attributed to the macropores with aperture > 300 nm and the outer surface, in which the high acidic groups (3.6 meq g^{-1}) of AC400 favored the adsorption of alkaline MB. The adsorption of MB on the outer surface was confirmed by the SEM spectra, as the surface of MB-adsorbed AC400 was much smoother as compared with that of AC400 (see Fig. 1). The adsorption of MB on the AC400 was also qualitatively reflected by the FT-IR analysis (see Fig. 6). Compared with the AC400, the MB-adsorbed AC400 had additional peaks at 1380 and 1320 cm^{-1}, related to the methyl groups of MB.

3.2.2 Adsorption kinetics and isotherm

After an integrated consideration of the activated carbon yield, pyrolysis temperature, BET surface area, pore volume, and MB adsorption capacity, AC400 was selected as the preferred one and it was used for further adsorption kinetics and isotherm studies. Information of kinetics is very important for modeling the adsorption process, as well as for both economic and industrial applications. Since AC400 has a high adsorption capability, relative high initial MB concentrations, i.e., 1000, 1500, and 2000 mg/L, were used for the kinetics studies. The influence of contact time on MB adsorption is shown in Fig. 7. The saturation curves rise sharply at initial stages and the curves level off with contact time, and a plateau of all curves occurs when the MB adsorption reached equilibrium. Longer contact time for equilibrium was required for MB solutions with higher initial concentration. It seems that contact time for the equilibrium required approximately 3 h, 12 h, and 24 h for MB solutions with initial concentrations of 1000 mg/L, 1500 mg/L, and 2000 mg/L, respectively. The adsorption capacity at equilibrium (q_e) increased from 592 to1085 mg/g when the initial MB concentrations increased from 1000 to 2000 mg/L.

Table 2 listed the data of pseudo-first-order and pseudo-second-order kinetic models. The pseudo-second-order model indicates the adsorption is a chemisorption process through sharing or exchanging of electron between the solvent and the sorbate. The pseudo-first-order model means the adsorption rate based on the adsorption capacity [32–34]. The correlation coefficient R^2 and $\triangle q$ were 1.000 and 6–10 for pseudo-second-order kinetic model, and 0.7769–0.9572 and 84–93 for pseudo-first-order kinetic model, respectively. In addition, the $q_{e,cal}$ calculated by the pseudo-second-order model is in good agreement with $q_{e,exp}$, while the $q_{e,cal}$ calculated from the pseudo-first-order kinetic model is significantly different from the $q_{e,exp}$. All these R^2, $\triangle$q, and the difference between $q_{e,cal}$ and $q_{e,exp}$ confirmed that the MB adsorptions are better simulated by the pseudo-second-order kinetic model.

Table 2 The parameters for the pseudo-first-order and pseudo-second-order kinetic models

C_0 (mg/L)	$q_{e,\ exp}$ (mg/g)	Pseudo-first-order kinetic model				Pseudo-second-order kinetic model			
		k_1 (min^{-1})	$q_{e,\ cal}$ (mg/g)	$\triangle q$ (%)	R^2	k_2 (g/mg min)	$q_{e,\ cal}$ (mg/g)	$\triangle q$ (%)	R^2
1000	592.4	0.0211	170.6	84	0.7522	0.00043	592.8	6	1.000
1500	883.6	0.0054	248.8	92	0.8814	0.00013	887.8	9	1.000
2000	1084.5	0.0042	320.3	93	0.8656	0.000084	1087.7	10	1.000

Table 3 Isotherm parameters of Langmuir and Freundlich models

Langmuir isotherm				Freundlich isotherm		
q_m (mg/g)	K_L (L/mg)	R^2	R_L[a]	K_F	n_F	R^2
1125	0.137	1.000	3.64×10^{-3} (7.25×10^{-3})	5.68	0.212	0.8696

[a] The R_L outside and inside the bracket were calculated at the initial concentration of 2000 mg/L and 1000 mg/L, respectively

Langmuir and Freundlich models are used to investigate the adsorption process, and the parameters are listed in Table 3. Generally, the Langmuir model describes a homogenous surface adsorption, and Freundlich isotherm describes heterogeneous adsorption systems considering multilayer adsorption and interactions between the molecules adsorbed [25, 35].

The n_F in the Langmuir isotherm equation can be used to determine whether the adsorption is a typical chemical ($n_F < 1$) or a favorable physical process ($n_F > 1$) [32]. The n_F is 0.212, indicating that adsorption process tends to be the former. The correlation coefficients R^2 of Langmuir isotherm and Freundlich isotherm are 1.000 and 0.8696, respectively, indicating that the adsorption behavior complies with the Langmuir isotherm model better. The adsorption process is also interpreted by R_L, as the adsorption isotherm can be classified by unfavorable ($R_L > 1$), favorable ($0 < R_L < 1$), linear ($R_L = 1$), and irreversible ($R_L = 0$). The R_L is between 3.64×10^{-3} and 7.25×10^{-3} (see Table 3) when the initial MB concentration is 1000–2000 mg L^{-1}, indicating the adsorption process is favorable. Based on the calculation by Langmuir isotherm, the maximum adsorption capacity of the MB was 1125 mg/g. This adsorption capacity is quite high as compared with the MB adsorption capacity reported by previous works [22, 23, 32, 34].

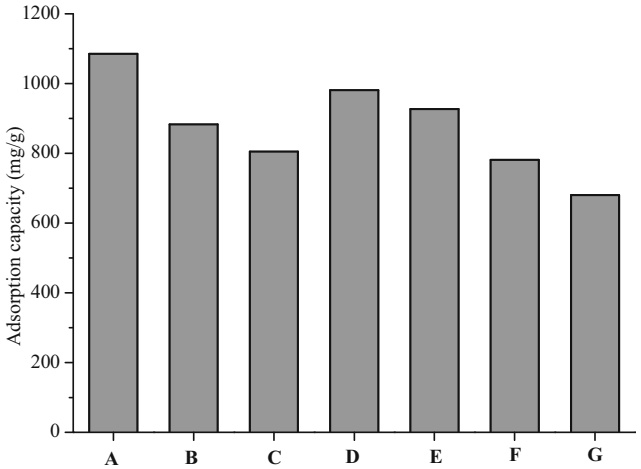

Fig. 8 Adsorption capacity of fresh AC400 and regenerated AC400. The used AC400 was regenerated by solvent extraction with a Soxhlet extractor for 24 h. A, fresh AC400; B, regenerated AC400 by methanol extraction for the 1st time; C, regenerated AC400 by acetone extraction for the 1st time; D, regenerated AC400 by DCM extraction for the 1st time; E, regenerated AC400 by DCM extraction for the 2nd time; F, regenerated AC400 by DCM extraction for the 3rd time; G, regenerated AC400 by DCM extraction for the 4th time

3.3 Desorption

A conventional method, extraction of MB by low-boiling point organic solvents (methanol, acetone, and DCM) in a Soxhlet extractor, was employed for a preliminary desorption study. After the first time extraction by methanol, acetone, and DCM, the adsorption capacity of regenerated AC400 was 883 mg/g, 805 mg/g, and 981 mg/g, respectively (see Fig. 8). It is therefore suggested that DCM was the best extraction solvent, and the regeneration resulted in decrease of adsorption capacity. The decrease of adsorption capacity after the regeneration can be explained by the FT-IR analysis (Fig. 6). The adsorbed AC400 had two obvious peaks at 1320 and 1380 cm^{-1}, owing to the methyl groups of MB. The two peaks were still observed on the regenerated AC400, though the intensity of the two peaks was much weaker than that of MB-adsorbed AC400, indicating that a small part of MB remained on the regenerated AC400. Although the adsorption capacity of regenerated AC400 decreased with the increased reuse times, a relative high adsorption capacity of 680 mg/g was observed in reusing the AC400 for five times (see Fig. 8).

4 Conclusion

In this work, value-added application of biomass hydrolysis-derived humins for activated carbon production was achieved by H_3PO_4 activation method. The activated carbons owned amorphous carbon and aromatic structures, with the yield, total acidity, BET surface area, and BJH pore volume of 51.9–73.5 wt%, 3.3–3.7 meq g^{-1}, 1358–2375 m^2/g, and 0.25–0.88 cm^3/g, respectively. Pyrolysis temperature is an important factor affecting the activated carbons' properties, and 400 °C was found as an optimum temperature for the preparation of high-performance AC400, exhibiting highest BET surface area, BJH pore volume, and MB adsorption capacity. The adsorption of MB on AC400 complied with the pseudo-second-order kinetics, and an outstanding Langmuir adsorption capacity of 1125 mg/g was calculated. Moreover, the used AC400 could be simply regenerated by organic solvent Soxhlet extraction method, and a comparable adsorption capacity of 680 mg/g was maintained for fifth reusing. The good adsorption and desorption properties of the AC400 confirmed that the valorization of humins by phosphoric acid activation process is an effective and promising technology.

Funding information This article was made possible by Grant Number 21606045 from the National Natural Science Foundation of China and by Grant Number 2017A030313084 from the Natural Science Foundation of Guangdong Province of China, and Guangdong Innovation Research Team for Higher Education (2017KCXTD030).

References

1. Kang S, Fu J, Zhang G (2018a) From lignocellulosic biomass to levulinic acid: a review on acid-catalyzed hydrolysis. Renew Sust Energ Rev 94:340–362
2. Rout PK, Nannaware AD, Prakash O, Kalra A, Rajasekharan R (2016) Synthesis of hydroxymethylfurfural from cellulose using green processes: a promising biochemical and biofuel feedstock. Chem Eng Sci 142:318–346
3. Bozell JJ (2010) Connecting biomass and petroleum processing with a chemical bridge. Science 329:522–523
4. Galletti AMR, Antonetti C, De Luise V, Licursi D, Nassi N (2012) Levulinic acid production from waste biomass. BioResour 7:1824–1835
5. Kang S, Yu J (2016) An intensified reaction technology for high levulinic acid concentration from lignocellulosic biomass. Biomass Bioenergy 95:214–220
6. Patil SK, Heltzel J, Lund CR (2012) Comparison of structural features of humins formed catalytically from glucose, fructose, and 5-hydroxymethylfurfuraldehyde. Energ Fuel 26:5281–5293
7. van Zandvoort I, Wang Y, Rasrendra CB, van Eck ER, Bruijnincx PC, Heeres HJ, Weckhuysen BM (2013) Formation, molecular structure, and morphology of humins in biomass conversion: influence of feedstock and processing conditions. ChemSusChem 6: 1745–1758
8. Ordomsky V, Sushkevich V, Schouten J, Van Der Schaaf J, Nijhuis T (2013) Glucose dehydration to 5-hydroxymethylfurfural over phosphate catalysts. J Catal 300:37–46
9. Sumerskii I, Krutov S, Zarubin MY (2010) Humin-like substances formed under the conditions of industrial hydrolysis of wood. Russian J Appl Chem 83:320–327
10. Weingarten R, Conner WC, Huber GW (2012) Production of levulinic acid from cellulose by hydrothermal decomposition combined with aqueous phase dehydration with a solid acid catalyst. Energy Environ Sci 5:7559–7574
11. Rasrendra CB, Windt M, Wang Y, Adisasmito S, Makertihartha IGBN, van Eck ERH, Meier D, Heeres HJ (2013) Experimental studies on the pyrolysis of humins from the acid-catalysed dehydration of c6-sugars. J Anal Appl Pyrol 104:299–307
12. Hoang TM, Lefferts L, Seshan K (2013) Valorization of humin-based byproducts from biomass processing-a route to sustainable hydrogen. Chemsuschem 6:1651–1658
13. Kang S, Zhang G, Yang Q, Tu J, Guo X, Qin FG, Xu Y (2016) A new technology for utilization of biomass hydrolysis residual humins for acetic acid production. BioResour 11:9496–9505
14. Pin JM, Guigo N, Mija A, Vincent L, Sbirrazzuoli N, van der Waal J, de Jong E (2014) Valorization of biorefinery side-stream products: combination of humins with polyfurfuryl alcohol for composite elaboration. ACS Sustain Chem Eng 2:2182–2190
15. Kang S, Fu J, Zhang G, Zhang W, Yin H, Xu Y (2017) Synthesis of humin-phenol-formaldehyde adhesive. Polymers 9(8):373
16. Girisuta B, Janssen L, Heeres H (2006) A kinetic study on the decomposition of 5-hydroxymethylfurfural into levulinic acid. Green Chem 8:701–709
17. Girisuta B, Janssen L, Heeres H (2007) Kinetic study on the acid-catalyzed hydrolysis of cellulose to levulinic acid. Ind Eng Chem Res 46:1696–1708
18. Kang S, Fu J, Deng Z, Jiang S, Zhong G, Xu Y, Guo J, Zhou J (2018b) Valorization of biomass hydrolysis waste: activated carbon from humins as exceptional sorbent for wastewater treatment. Sustainability 10:1795
19. Zheng W, Bao W, Gu B, He X, Leng L (2007) Carbon concentration and its characteristics in terrestrial higher plants. Chin J Ecol 26:307–313
20. Ioannidou O, Zabaniotou A (2007) Agricultural residues as precursors for activated carbon production—a review. Renew Sust Energ Rev 11:1966–2005
21. Guan W, Xu G, Duan J, Shi S (2018) Acetone–butanol–ethanol production from fermentation of hot-water-extracted hemicellulose hydrolysate of pulping woods. Ind Eng Chem Res 57:775–783
22. Altenor S, Carene B, Emmanuel E, Lambert J, Ehrhardt JJ, Gaspard S (2009) Adsorption studies of methylene blue and phenol onto vetiver roots activated carbon prepared by chemical activation. J Hazardous Mater 165:1029–1039
23. Jamion N, Hashim I (2017) Preparation of activated carbon from tamarind seeds and methylene bule (MB) removal. J Fundamen Appl Sci 9:102–114
24. Kang S, Li X, Fan J, Chang J (2012) Characterization of hydrochars produced by hydrothermal carbonization of lignin, cellulose, d-xylose, and wood meal. Ind Eng Chem Re 51:9023–9031
25. Hameed B, Rahman A (2008) Removal of phenol from aqueous solutions by adsorption onto activated carbon prepared from biomass material. J Hazardous Mater 160:576–581
26. Solum MS, Pugmire RJ, Jagtoyen M, Derbyshire F (1995) Evolution of carbon structure in chemically activated wood. Carbon 33:1247–1254
27. Jagtoyen M, Derbyshire F (1998) Activated carbons from yellow poplar and white oak by H_3PO_4 activation. Carbon 36:1085–1097
28. Daletou MK, Geormezi M, Vogli E, Voyiatzis GA, Neophytides SG (2014) The interaction of H_3PO_4 and steam with PBI and TPS polymeric membranes. A TGA and Raman study. J Mater Chem A 2:1117–1127
29. Kang S, Yu J (2015) A gasoline-grade biofuel formed from renewable polyhydroxybutyrate on solid phosphoric acid. Fuel 160:282–290
30. Wang X, Huang A, Zhong S, Pan Y, Tian Y (2015) Facile preparation of mesoporous carbon microspheres containing nickel nanoparticle and dye adsorption behavior. Sci Adv Mater 7:43–49
31. Dehghani MH, Mostofi M, Alimohammadi M, McKay G, Yetilmezsoy K, Albadarin AB, Heibati B, AlGhouti M, Mubarak N, Sahu J (2016) High-performance removal of toxic phenol by single-walled and multi-walled carbon nanotubes: kinetics, adsorption, mechanism and optimization studies. J Ind Eng Chem 35:63–74
32. Vargas AM, Cazetta AL, Kunit MH, Silva TL, Almeida VC (2011) Adsorption of methylene blue on activated carbon produced from flamboyant pods (Delonix regia): study of adsorption isotherms and kinetic models. Chem Eng J 168:722–730
33. Gürses A, Doğar Ç, Yalçın M, Açıkyıldız M, Bayrak R, Karaca S (2006) The adsorption kinetics of the cationic dye, methylene blue, onto clay. J Hazardous Mater 131:217–228
34. Al-Ghouti MA, Khraisheh MA, Ahmad MN, Allen S (2009) Adsorption behaviour of methylene blue onto Jordanian diatomite: a kinetic study. J Hazardous Mater 165:589–598
35. El Qada EN, Allen SJ, Walker GM (2006) Adsorption of methylene blue onto activated carbon produced from steam activated bituminous coal: a study of equilibrium adsorption isotherm. Chem Eng J 124:103–110